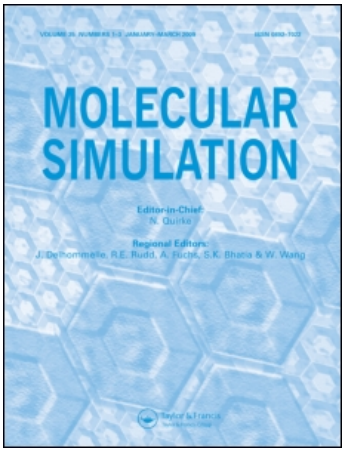

Molecular Simulation
Publication details, including instructions for authors and subscription information:
http://www.informaworld.com/smpp/title~content=t713644482

Chaotic flows in microchannels: a lattice Boltzmann study

F. Varnik[a]; D. Raabe[a]
[a] Max-Planck Institut für Eisenforschung, Düsseldorf, Germany

To cite this Article Varnik, F. and Raabe, D.(2007) 'Chaotic flows in microchannels: a lattice Boltzmann study', Molecular Simulation, 33: 7, 583 — 587
To link to this Article: DOI: 10.1080/08927020601030456
URL: http://dx.doi.org/10.1080/08927020601030456

Molecular Simulation, Vol. 33, No. 7, June 2007, 583–587

Taylor & Francis
Taylor & Francis Group

Chaotic flows in microchannels: a lattice Boltzmann study

F. VARNIK* and D. RAABE

Max-Planck Institut für Eisenforschung, Max-Planck Straße 1, 40237 Düsseldorf, Germany

(Received July 2006; in final form September 2006)

Roughness effects on lubricant flows are investigated via 2D lattice Boltzmann simulations. At a Reynolds numbers of order 1000 a transition from laminar to unsteady flow is observed by an increase of the roughness height from about 10% to about 25% of the channel width. At lower Reynolds numbers (where the flow is laminar in both channels), the transition is observed when increasing the wall roughness further. In other words, the critical Reynolds number for the transition from laminar toward unsteady flow decreases at higher wall roughness. Wall roughness may, therefore, qualitatively change the flow properties in confined geometry. Due to the ubiquitous presence of the wall roughness, the phenomenon is relevant in all cases where relatively high Reynolds number flow occur in strongly confined channels such as lubricant flow during the deformation of solid surfaces. For a fixed Reynolds number and channel geometry, time and spatial dependence of the velocity field and fluctuating quantities obey the scaling behavior as expected from the structure of the Navier–Stokes (NS) equations. This underlines the physical significance of the observed transition. As a possible application, wall roughness may be used in order to enhance mixing efficiency at a given Reynolds number.

Keywords: Lattice Boltzmann method; Chaotic mixing; Flow at rough surfaces; Flow instability

1. Introduction

Fluid mechanics at deformable metallic surfaces has long been studied within the framework of classical continuum-based metal/fluid tribology theory and macroscopic engineering experimentation in the context of sheet metal forming [1]. Since the last decade, more attention has been paid to the study fluid mechanics at deformable metallic surfaces also at the molecular dynamics scale [1].

Both methods of tackling fluid mechanics at deformable metallic surfaces are characterized by several limitations. The first set of limitations associated with conventional macroscopic continuum-based approaches along these lines lies in the scale. Classical works about tribology at metal/fluid interfaces which take a continuum perspective study fluid dynamics at the macroscopic or, respectively, statistical scale [1].

This means that fluid flow is usually assumed to be laminar and the metallic surface is anticipated to be perfectly flat. Both assumptions must be modified when it comes to a detailed analysis. Firstly, we recall that fluid velocities of order 100 m/s (7% of the sound speed in water) or higher are quite common in rapid quenching processes [2]. Taking a channel of width 100 μm and a dynamic viscosity of $\nu = 10^{-5}$ (oil) yields Reynolds numbers of order $Re \sim 1000$. On the other hand, metallic surfaces are never flat but reveal an average roughness ranging from some nanometers to some tens of micrometers depending on the mechanical and microstructural boundary conditions. This applies in particular to the evolution of surface roughness during elastic–plastic deformation.

In a recent publication [3], we have shown that, when these two facts (relatively high Reynolds number and non-negligible wall roughness) are combined together, a new kind of unsteady flow behavior occurs which is different from rough wall turbulence [4]. Contrary to the latter, where the flow is turbulent also over a flat surface, the case studied in Ref. [3] is marked by a transition from a laminar towards an unsteady flow as the wall roughness gradually increases.

Note that an unsteady flow is not necessarily chaotic. It may, for example, be a superposition of simple oscillatory modes with a distribution of amplitudes depending on the channel geometry, the wall roughness and the Reynolds number. In the present work, we are going to show that it is indeed possible to create fully chaotic flows by a proper design of the channel geometry while keeping the Reynolds number constant.

*Corresponding author. Email: varnik@mpie.de

Molecular Simulation
ISSN 0892-7022 print/ISSN 1029-0435 online © 2007 Taylor & Francis
http://www.tandf.co.uk/journals
DOI: 10.1080/08927020601030456

2. Simulation method

The lattice Boltzmann method (LBM), a kinetic approach to solve the Navier–Stokes (NS) equation is used. While direct derivations of the method now exist, the LBM has been historically devised as an improvement of the lattice gas cellular automata (LGCA) [5–10] providing, e.g. a far better statistical accuracy [10–12]. In the past 20 years, the LBM has been extensively used as an efficient tool for the study of a variety of fluid flow problems such as two-phase flow through porous media [13], particle-fluid suspensions [14,15] and high Reynolds number turbulent flows [16].

There are excellent monographs [17–19] and comprehensive review articles [20,14,21] on the LBM and the historically related LGCA. Here, we give a short introduction of the method. A simplified view of the LBM may be presented as follows: A fluid portion residing at a given point, $\mathbf{x}$, in space is divided into a small number of parcels, f_i, each moving with a well defined velocity, $\mathbf{c}_i$, on a lattice (figure 1).

A single-time BGK scheme [22] is used for the relaxation step. During the time step $t \rightarrow t+1$ (note that $\Delta t = 1$), the fluid parcel, $f_i(\mathbf{x}, t)$, is first relaxed to its local equilibrium, $f_i^{\mathrm{eq}}(\mathbf{x}, t)$, with a rate of ω

$$f_i'(\mathbf{x}, t) = f_i(\mathbf{x}, t) - \omega(f_i(\mathbf{x}, t) - f_i^{\mathrm{eq}}(\mathbf{x}, t)), \qquad (1)$$

and then freely propagated to the site $\mathbf{x} + \mathbf{c}_i$

$$f_i(\mathbf{x} + \mathbf{c}_i, t+1) = f_i'(\mathbf{x}, t). \qquad (2)$$

Here, the post-collision population, f_i' is introduced to underline the formal separation of the relaxation and propagation steps. The relaxation rate is closely related to the fluid dynamic viscosity via

$$\nu = \frac{1}{6}\left(\frac{2}{\omega} - 1\right). \qquad (3)$$

The local equilibrium distribution, f_i^{eq}, is usually taken as a second order expansion of the Maxwell velocity distribution leading to

$$f_i^{\mathrm{eq}} = \rho w_i \left[1 + \frac{1}{c_s^2}\mathbf{u}\cdot\mathbf{c}_i + \frac{1}{2c_s^4}\left[(\mathbf{u}\cdot\mathbf{c}_i)^2 - c_s^2\mathbf{u}\cdot\mathbf{u}\right]\right], \qquad (4)$$

where c_s is the sound speed and w_i is a set of weights normalized to unity. For the two dimensional nine velocity model (D2Q9) used in our studies (see figure 1 for an illustration) one finds $w_0 = 4/9$, $w_1 = w_2 = w_3 = w_4 = 1/9$ and $w_5 = w_6 = w_7 = w_8 = 1/36$ (see Ref. [19] for a short but comprehensive derivation). Once the discrete populations, f_i, are known, fluid density, $\rho(\mathbf{x}, t)$, and velocity, $\mathbf{u}(\mathbf{x}, t)$, at a given point and time are obtained via

$$\rho = \sum_i f_i(\mathbf{x}, t) \quad \text{and} \quad \rho\mathbf{u} = \sum_i f_i(\mathbf{x}, t)\mathbf{c}_i. \qquad (5)$$

For the fluid–solid interaction, the bounce-back rule is used: fluid populations arriving at a solid node are sent back to the node where they came from. At not too high viscosities, this leads to zero streaming velocity half-way between a solid node and its neighboring fluid node (stick boundary condition). In the following, all quantities are expressed in lattice Boltzmann (LB) units. The unit of length is the internode spacing, $\Delta x \equiv 1$. The time in measured in units of an iteration step, $\Delta t \equiv 1$. This fixes the unit of the velocity $\Delta x/\Delta t \equiv 1$. Comparison with real experiments is easily done by, e.g. fixing the dynamic viscosity, ν, and the sound speed c_s.

At high dynamic viscosities, the bounce back rule is not able to perfectly ensure the stick boundary condition and a partial slip at the walls occurs [24,3]. This finite slip is closely related to the kinetic nature of the LB method and brings about the relevance of Knudsen issues for the problem under consideration. The Knudsen number (Kn = mean free path/characteristic length) is a measure of the validity of the hydrodynamic limit for the problem of interest (the lower Kn, the better this limit is approached). The Knudsen number associated with a lattice pitch is given by $Kn(\Delta x) = l/\Delta x = \nu/c_s$ [3]. Noting that c_s is usually of order unity ($c_s = 1/\sqrt{3} \approx 0.6$ for the two dimensional nine velocity model used in this work) it follows that the largest Knudsen number occurring in the problem is of order the dimensionless dynamic viscosity, ν (we assume that the problem does not contain length scales smaller than Δx). As a consequence, $Kn(\Delta x) > 1$ for $\nu > 1$. In other words, the basic requirement of low Knudsen number is violated at LB dynamic viscosities of order unity or higher. However, all the simulations reported here are performed at $\nu \leq 0.001$ thus ensuring the validity of hydrodynamic limit.

As can be seen from the above description, the solution for the particle distribution function, f_i, is explicit and local. The corresponding code is, therefore, easy to implement, locality being a precondition for an efficient parallelization. Furthermore, within the LBM, any point on the lattice can be defined as a solid node thus providing a simple framework for the simulation of the flow in arbitrarily complex geometries. A further advantage of LB

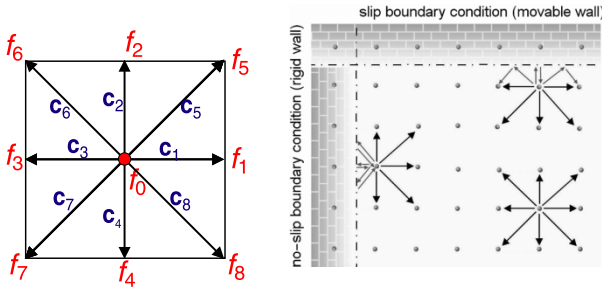

Figure 1. Left, schematic view of two dimensional nine velocity (D2Q9) lattice Boltzmann model. During the free propagation step, the population f_i is transported along the velocity vector $\mathbf{c}_i$. The zero-velocity population, f_0, ensures correct hydrodynamic behavior in the compressible regime, i.e. at high mach numbers (fluid velocity/sound speed). Right, illustration of rules in order to realize stick or slip boundary conditions.

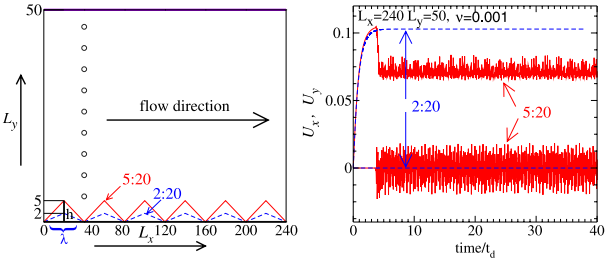

Figure 2. Left, a sketch of the simulation box for two choices of the wall roughness. The top wall is assumed to be flat, whereas the bottom wall has a zig-zag form. A zig-zag wall can be characterized by two numbers: the height, h, of the roughness tip and the half-wave length $\lambda/2$. We use the notation $h{:}\lambda/2$ for a given zig-zag wall. Flow velocity versus time is recorded at equidistant points along the line $x = 40$ (open circles). Note that the region below the zig-zag line is filled with solid particles (not shown for clarity). Right, parallel, U_x, and the perpendicular, U_y, components of the fluid velocity in the middle of the flow region versus time for both choices of the wall roughness shown in the left panel. The time axis is rescaled by the momentum diffusion time. Note the strong fluctuations of the *vertical* component of the velocity in the case of the 5:20 zig-zag surface.

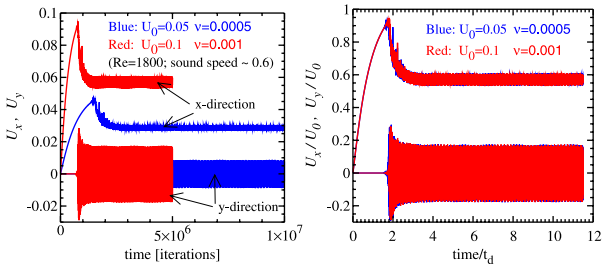

Figure 3. Scaling behavior of the velocity field. Left, horizontal, U_x, and vertical, U_y, components of the streaming velocity are shown versus time for two choices of the parameter U_0 (the external force is set such that, in the case of a laminar flow, the mid-channel velocity would equal U_0). Left, Same as in the left panel, but rescaled. U_x and U_y are divided by the characteristic flow velocity, U_0, and the time is given in units of the momentum diffusion time, t_d.

over a purely hydrodynamic description is the fact that the fluid pressure and the stress tensor are available on each lattice node with no need of solving a computationally demanding Poisson problem. Finally, recent developments such as grid-refinement and finite-volume approaches allow to considerably increase computational efficiency and accuracy when simulating situations of engineering interest [23] thus making the LB approach an attractive candidate for tackling complex fluid dynamic problems.

3. Results

Figure 2 illustrates how a variation of the surface roughness alone may trigger transition toward unsteady flow. In the right panel of the figure, velocity versus time is shown for two choices of the wall roughness as described in the left panel. Here, horizontal, U_x and vertical, U_y, components of the fluid velocity are monitored at a fixed point in the middle of the flow region. The time axis is rescaled by the momentum diffusion time $t_d = H^2/(8\nu)$ (H = effective channel width) as can be estimated from a study of the Stokes flow in the same channel with parallel walls.

The fluid is at rest for $t < 0$. At $t = 0$ an external body force is switched on, which accelerates the fluid gradually toward a steady state flow†. In the channel with a 2:20 zig-zag surface, the fluid velocity in the direction parallel to the wall, U_x, increases continuously and smoothly until it reaches a constant value after a time of order t_d while the vertical component of the velocity, U_y, remains zero for all times.

A qualitative change in the flow behavior is, however, observed as the roughness height is increased from 2 to 5 lattice units (corresponding to a change of the roughness slope from 0.1 to 0.25 at the same roughness wave length). Now, both U_x and U_y exhibit strong fluctuations suggesting the presence of flow instability. A further hint on flow instability is the observed drop of the mean velocity at the onset of fluctuations, indicative of a higher rate of energy loss (and thus a higher friction force) due to the chaotic nature of the flow.

It must be emphasized here that the roughness-induced flow instability discussed above is not restricted to the specific choice of triangular obstacles. We do observe the same phenomenon also for a variety of other regular surfaces as well as for a random distribution of roughness elements.

In order to examine the physical significance of the observed transition we have computed various quantities for which exact behavior can be derived from the NS equation. An example is the sum of the viscous stress $\nu\rho\partial\langle U_x\rangle/\partial y$ and the so-called Reynolds stress $-\rho\langle\delta U_x\delta U_y\rangle$ which obeys a straight line with an slope, ρg, (g = imposed external force per unit mass): $\nu\rho\langle\partial U_x/\partial y\rangle - \rho\langle u_x u_y\rangle = \tau_w + \rho g(y - y_w)$ (y_w = the position of the wall, τ_w = viscous stress at the wall). Indeed, this equation is very well satisfied by our simulation results [2].

A further, non-trivial, hint regarding the reliability of simulated results is to verify whether the solutions obtained within our simulations obey scaling rules as expected from the structure of the NS-equations: For a given Reynolds number and channel geometry the solution of the NS-equation is unique if expressed in appropriate dimensionless units. As shown in figures 3 and 4, the solutions obtained within our simulations satisfy this important requirement.

The test shown in figure 4 also provides useful information on the accuracy of the results with respect to the grid resolution. If the grid resolution was not satisfactory in order to capture the basic physics of the problem, a significantly different behavior could be observed when comparing results for different system sizes. Indeed, a close

†Note that we apply the term "steady state" not only for a time independent flow, but also for a time dependent flow, whose statistical properties do not change with time.

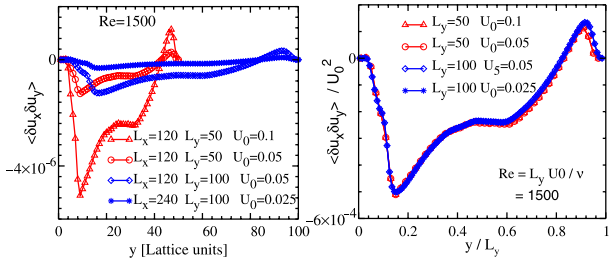

Figure 4. Scaling property of the Reynolds stress, $\tau_{\text{rey}} = \langle \delta U_x \delta U_y \rangle (\delta U = U - \langle U \rangle)$. τ_{rey} is computer for different channel sizes and velocities as indicated in the figure while both the channel shape and the Reynolds number were kept unchanged. Right panel shows the same quantities now rescaled appropriately.

inspection of the right panel of figure 4 reveals some small deviations when changing the system size, whereas, for a given system size, the rescaled Reynolds stresses obtained for different characteristic velocities are identical. These deviations are, however, quite small compared to the overall variation of the Reynolds stress. This observation strongly suggests that, even in the case of the smallest system studied ($L_x \times L_y = 120 \times 50$), our simulation results are accurate enough in order to describe the essential features of the studied phenomenon.

Next we address the question whether a fully chaotic flow may be achieved by modifying the channel geometry alone, i.e. by keeping the Reynolds number (nearly) constant. A way to visualize the chaoticity of a flow is to add passive tracer particles to the flow and to survey the time evolution of the tracer field. Passive tracers have the advantage of following the flow without perturbing it. The time evolution of a passive tracer pattern thus reflects the genuine flow dynamics. Within the LB approach, tracer particles are added by introducing a new population density, $g_i, i = 0, 1, \ldots, 8$. The tracer variables g_i obey the same relaxation and propagation steps as their fluid counterpart f_i. In particular,

$$g_i'(\mathbf{x}, t) = g_i(\mathbf{x}, t) - \omega_{\text{tracer}}(g_i(\mathbf{x}, t) - g_i^{\text{eq}}(\mathbf{x}, t)), \quad (6)$$

and

$$g_i(\mathbf{x} + \mathbf{c}_i, t + 1) = g_i'(\mathbf{x}, t). \quad (7)$$

ω_{tracer} is closely related to the tracers dynamic viscosity (and hence to tracer diffusivity) ν_{tracer} via the analog of equation (3),

$$\nu_{\text{tracer}} = \frac{1}{6}\left(\frac{2}{\omega_{\text{tracer}}} - 1\right). \quad (8)$$

However, compared to f_i which fully determine f_i^{eq} via equations (4) and (5), g_i enters g_i^{eq} only through the prefactor $\rho_{\text{tracer}} = \sum_i g_i(\mathbf{x}, t)$. Indeed, g_i^{eq} is mainly determined by the flow velocity u (and thus by f_i) via

$$g_i^{\text{eq}} = \rho_{\text{tracer}} w_i \left[1 + \frac{1}{c_s^2}\mathbf{u}\cdot\mathbf{c}_i + \frac{1}{2c_s^4}\left[(\mathbf{u}\cdot\mathbf{c}_i)^2 - c_s^2\mathbf{u}\cdot\mathbf{u}\right]\right]. \quad (9)$$

The above equations ensure that the tracer is advected by the flow without any impact on the flow properties.

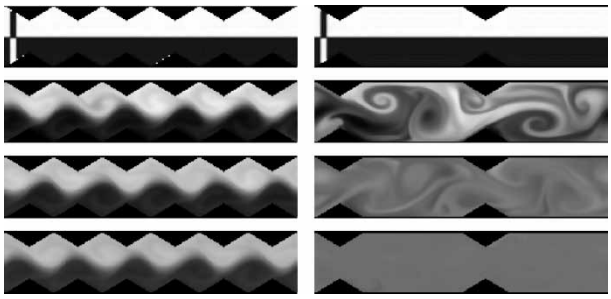

Figure 5. Impact of the channel design on the chaotic nature of the flow. In a zig-zag channel (left), 2/3 of all "teeth" are removed (right). The chaotic nature of the flow is visualized by filling the bottom half of the channel by a passive tracer (dark color). A thin vertical slab of the tracer at the entrance of the channel is also added in order to visualize the stream wise fluid motion. This thin slab disperses fast compared to the time scale resolved here. The time from top to bottom $t = 10, 10^4, 2 \times 10^4, 3 \times 10^4$ (in LB units). Obviously, the chaotic nature of the flow is significantly enhanced by the removal of obstacles. Note also that in the case shown here the time necessary for mixing through diffusion is about $t_{\text{diff}} = 3 \times 10^5$, i.e. by a factor of hundred larger than the latest time shown. The observed mixing is, therefore, fully due to the chaotic nature of the flow.

Using this algorithm, simulations are performed for various Reynolds numbers and roughness types for which a transition towards instability was observed. First, we simulate the flow in a given channel until it reaches a steady state in the sense that its statistical properties no longer depend on time. Then we reset the time clock to zero and add a tracer field to the bottom half of the channel. The simulation then goes on while monitoring the dynamic of the tracer field via equations (6)–(9). During this part of the simulation, the tracer distribution is saved on hard disk in regular time intervals allowing an analysis of the data at the end of the simulation.

A typical result of these simulations is shown in figure 5, where the tracer field (dark color) at various times is shown in two channels differing in the wall geometry only, all the other parameters of the simulation such as the average flow velocity ($\bar{u} \approx 0.025$) and the Reynolds number ($Re = \bar{u}H/(2\nu) \approx 625$ using the channel width $H = 50$ and $\nu = 0.001$) being nearly identical. The time increases from top to bottom as $t = 10, 10^4, 2 \times 10^4, 3 \times 10^4$. Note that the flow is unsteady in the case of the both channel geometries shown. Nevertheless, the flow exhibits quite different degrees of chaoticity depending on the channel geometry. Interestingly, the unstable character of the flow is enhanced by the removal of obstacles. In other words a dense array of obstacles may even *stabilize* the flow.

4. Summary

Results of LB simulations on roughness-induced transition toward an unsteady flow are presented. The work is motivated by the fact that relatively high Reynolds number flows may occur in narrow channels in a variety of situations. The term "relatively high", here, means that we consider situations where the non linear term in the NS equation is no longer negligible, but the flow remains laminar and stable with respect to small perturbations. This

brings about the relevance of the wall-roughness as an independent parameter affecting the flow properties: Wall roughness may serve as a source of large perturbations in the sense that these perturbations will not decay fast enough along the flow so that their advection with the flow can give rise to a complex and unsteady behavior.

In cases where the average roughness height is of order of 10% of the channel width or larger, we do indeed observe a crucial dependence of the flow on the wall roughness for Reynolds numbers of order 1000 [3]. The onset of unsteady flow is shifted toward lower Reynolds numbers as the roughness height is increased.

The physical significance of the obtained results is underlined by demonstrating that solutions obtained within the present simulations satisfy the scaling requirement of the NS equation: When all quantities such as velocity and the Reynolds stress are expressed in appropriate units, the solution is unique for all choices of the mean streaming velocity, system size, etc. provided that the Reynolds number and the channel shape are unaltered.

The phenomenon reported here is of particular importance in all cases where the roughness height is of the order of 10% the channel width or higher. An example of considerable importance is lubricant flow occurring during the deformation of solid surfaces.

Finally, we also give an example how an appropriate design of the channel geometry may considerably enhance the chaotic nature of the flow (figure 5). In view of increasing number of potential applications of chaotic flows [25] in civil engineering, environmental industry (e.g. solution recovery) as well as in the medical science (e.g. enhanced chaotic mixing in microchannels), the results of our studies may find a wide range of applications as they open an alternative way for tuning flow properties.

Acknowledgements

FV is supported by the DFG under the grants Do794/1-1 and Va205/3-2.

References

[1] N. Bay, T. Wanheim. Contact phenomena under bulk plastic deformation conditions. *Adv. Technol. Plast.*, **4**, 1677 (1990).
[2] F. Varnik, D. Raabe. Scaling effects in microscale fluid flows at rough solid surfaces. *Modell. Simul. Mater. Sci. Eng.*, **14**, 857 (2006).
[3] F. Varnik, D. Raabe. Roughness-induced flow instability: a lattice Boltzmann study. *J. Fluid Mech.*, **573**, 191 (2007).
[4] P.-A. Krogstad, R.A. Antonia. Surface roughness effects in turbulent boundary layers. *Exp. Fluids* **27**, 450 (1999); S. Pope, *Turbulent Flows* (Cambridge university press, Cambridge, UK, 2000); J. Mathieu and J. Scott, *An Introduction to Turbulent Flow* (Cambridge university press, Cambridge, UK, 2000).
[5] R. Benzi, S. Succi, M. Vergassola. The lattice-Boltzmann equation—theory and applications. *Phys. Rep.*, **3**, 145 (1992).
[6] L. Bunimovich, A. Lambert, R. Lina. The emergence of coherent structures in coupled map lattices. *J. Stat. Phys.* (1990).
[7] S. Chen, X. Shan, Z. Wang, G. Doolen. Lattice–Boltzmann computational fluid dynamics in three dimensions. *J. Stat. Phys.*, **68**, 379 (1992).
[8] U. Frisch, B. Hasslacher, Y. Pomeau. Lattice gas hydrodynamics in two and three dimensions. *Phys. Rev. Lett.*, **56**, 1505 (1986).
[9] F. Higuera, J. Jimenez. Boltzmann approach to lattice-gas simulations. *Europhys. Lett.*, **9**, 663 (1989).
[10] G. McNamara, G. Zanetti. Use of the Boltzmann equation to simulate lattice-gas automata. *Phys. Rev. Lett.*, **61**, 2332 (1988).
[11] F. Higuera, S. Succi, R. Benzi. Lattice gas dynamics with enhanced collisions. *Europhys. Lett.*, **9**, 345 (1989).
[12] Y. Qian, D. d'Humieres, P. Lallemand. Lattice BGK models for Navier–Stokes equation. *Europhys. Lett.*, **17**, 479 (1992).
[13] A. Gunstensen, D. Rothman. Lattice-Boltzmann studies of two-phase flow through porous media. *J. Geophys. Res.*, **98**, 6431 (1993).
[14] A. Ladd, R. Verberg. Lattice-Boltzmann simulations of particle-fluid suspensions. *J. Stat. Phys.*, **104**, 1191 (2001).
[15] P. Ahlrichs, B. Dünweg. Simulation of a single polymer chain in solution by combining lattice Boltzmann with molecular dynamics. *J. Chem. Phys.*, **111**, 8225 (1999).
[16] S. Succi, O. Filippova, H. Chen, S. Orszag. Towards a renormalized lattice Boltzmann equation for fluid turbulence. *J. Stat. Phys.*, **107**, 261 (2002).
[17] S. Succi. *The Lattice Boltzmann Equation: for Fluid Dynamics and Beyond (Series Numerical Mathematics and Scientific Computation)* (Oxford University Press, Oxford, 2001).
[18] D.H. Rothman, S. Zaleski. *Lattice–Gas Cellular Automata (Simple Models of Complex Hydrodynamics)* (Cambridge University Press, Cambridge, 1997).
[19] D. Wolf-Gladrow. *Lattice–Gas Cellular Automata and Lattice Boltzmann Models* (Springer, Berlin, Heidelberg, 2000).
[20] S. Chen, G. Doolen. Lattice Boltzmann method for fluid flows. *Ann. Rev. Fluid Mech.*, **30**, 329 (1998).
[21] D. Raabe. Overview of the lattice Boltzmann method for nano- and microscale fluid dynamics in materials science and engineering. *Modell. Simul. Mater. Sci. Eng.*, **12**, R13 (2004).
[22] P. Bhatnagar, E.P. Gross, M.K. Krook. A model for collision processes in gases. I. Small amplitude processes in charged and neutral one-component systems. *Phys. Rev.*, **94**, 511 (1954).
[23] S. Ubertini, S. Succi. Recent advances of lattice Boltzmann techniques on unstructured grids. *Prog. Comput. Fluid Dyn.* **5**, 85 (2005); O. Filippova and D. Hänel, Grid refinement for lattice BGK models, *J. Comp. Phys.* **147**, 219 (1998).
[24] R. Cornubert, D. h'Hummiières, D. Levermore. A Knudsen layer theory for lattice gases. *Physica D*, **47**, 241 (1991); L.S. Luo, Analytic solutions of linearized lattice Boltzmann equations for simple flows, *J. Stat. Phys.*, **88**, 913 (1997).
[25] C. Simonnet, A. Groisman. Chaotic mixing in a steady flow in a microchannel. *Phys. Rev. Lett.* **94**, 134501 (2005); A.D. Strook, S.K.W. Dertinger, A. Ajdari, I. Mezic, H.A. Stone, G.M. Whitesides, Chaotic mixer for microchannels, *Science*, **295**, 647 (2002); M.C. Jullien, P. Castiglione, P. Tabeling, Experimental observation of batchelor dispersion of passive tracers, *Phys. Rev. Lett.*, **85**, 3636 (2000); R.A. Truesdell, P.V. Vorobieff, L.A. Sklar, A.A. Mammoli, Mixing of a continuous flow of two fluids due to unsteady flow, *Phys. Rev. E*, **67**, 066304 (2003).